ACS Energy LETTERS

Cite This: ACS Energy Lett. 2018, 3, 125−131

LETTER

Tantalum Oxide Electron-Selective Heterocontacts for Silicon Photovoltaics and Photoelectrochemical Water Reduction

Yimao Wan,*[,∇,†,‡,§] Siva Krishna Karuturi,[∇,∥] Christian Samundsett,[†] James Bullock,[‡,§] Mark Hettick,[‡,§] Di Yan,[†] Jun Peng,[†] Parvathala Reddy Narangari,[∥] Sudha Mokkapati,[⊥] Hark Hoe Tan,[∥] Chennupati Jagadish,[∥] Ali Javey,[‡,§] and Andres Cuevas[†]

[†]Research School of Engineering, The Australian National University (ANU), Canberra, ACT 0200, Australia
[‡]Department of Electrical Engineering and Computer Sciences, University of California, Berkeley, California 94720, United States
[§]Materials Sciences Division, Lawrence Berkeley National Laboratory, Berkeley, California 94720, United States
[∥]Department of Electronic Materials Engineering, Australian National University (ANU), Canberra, ACT 0200, Australia
[⊥]School of Physics and Astronomy, Cardiff University, Cardiff, Wales, U.K.

Supporting Information

ABSTRACT: Crystalline silicon (c-Si) solar cells have been dominating the photovoltaic (PV) market for decades, and c-Si based photoelectrochemical (PEC) cells are regarded as one of the most promising routes for water splitting and renewable production of hydrogen. In this work, we demonstrate a nanoscale tantalum oxide (TaO_x, ~6 nm) as an electron-selective heterocontact, simultaneously providing high-quality passivation to the silicon surface and effective transport of electrons to either an external circuit or a water-splitting catalyst. The PV application of TaO_x is demonstrated by a proof-of-concept device having a conversion efficiency of 19.1%. In addition, the PEC application is demonstrated by a photon-to-current efficiency (with additional applied bias) of 7.7%. These results represent a 2% and 3.8% absolute enhancement over control devices without a TaO_x interlayer, respectively. The methods presented in this Letter are not limited to c-Si based devices and can be viewed as a more general approach to the interface engineering of optoelectronic and photoelectrochemical applications.

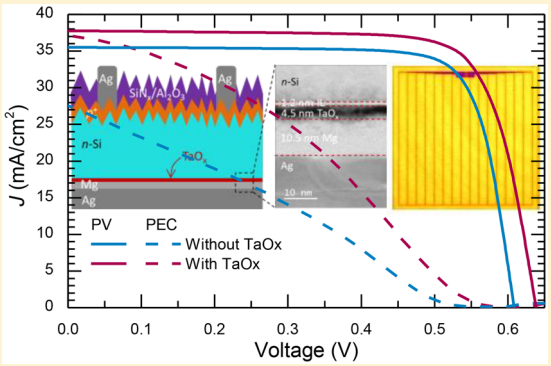

With increasing concerns over rising global energy demand and environmental sustainability, the development of renewable energy technologies is of great importance to the continuation of socio-economic development. There is growing consensus that significant contributions can come from the conversion of solar energy into electricity using photovoltaic (PV) cells[1] and/or into chemical energy using photoelectrochemical (PEC) devices.[2] With a 90% share of global PV market, crystalline silicon (c-Si) is unequivocally the most important photovoltaic technology. Because of its high abundance in the earth's crust and industrial maturity, c-Si based systems have also received significant attention for PEC applications.[3−7] Both PV and PEC devices rely on the same central working principle: photogenerated electrons and holes are separately collected at the two opposite terminals of the device. A common method to achieve this function is via doping (i.e., boron-doped p^+ or phosphorus-doped n^+) the near-surface regions of the silicon wafer or thin silicon films deposited on it.[8−10]

Another attractive approach to separately collect the two types of charge carriers is to use metal−insulator-semiconductor (MIS) passivated heterocontact structures. A typical MIS heterocontact is composed of a metal layer positioned on the outer surface of an oxide passivated semiconductor. To be able to function as passivated heterocontacts, the oxide interlayers have to fulfill several critical requirements: (i) effective passivation of defects typically present at the silicon surface, (ii) efficient transport of only one carrier type (for example electrons) and effective blocking of the other carrier (for example holes) in their path from the silicon photon absorber to the outer metal terminals, and (iii) simple synthesis

Received: November 20, 2017
Accepted: December 8, 2017

DOI: 10.1021/acsenergylett.7b01153
ACS Energy Lett. 2018, 3, 125−131

method at low thermal budget. Specific to PEC applications, the oxide interlayers also need to be chemically robust to survive in a very harsh aqueous environment for extended operation.

Ultrathin tunnelling silicon dioxide (SiO_2, typically ~1.5 nm) is one of the most explored oxides in heterocontacts for both PV[11,12] and PEC[4,6,13,14] applications because of its reasonable passivation quality and effective transport of carriers (i.e., permits the transport of majority carriers together with a low recombination of minority carriers)[11,12] and its stability over a wide range of pH and chemical potentials.[15] However, the highly insulating bulk properties of SiO_2 lead to inhibition of charge transport through the MIS heterocontacts, restricting conduction to tunnelling, or through pinholes. Furthermore, the high-quality ultrathin SiO_2 places stringent requirements in film thickness control and process environment purity. Profound efforts have been recently devoted to exploring alternatives to SiO_2 as the interlayer to form passivated carrier-selective heterocontacts on c-Si wafers, such as metal salts[16,17] and oxides[18] and organic polymers.[19,20]

Another group of candidate materials for MIS passivated heterocontacts are the transition-metal oxides, some of which possess almost all critical characteristics for carrier-selective contacts, including a wide range of work functions, semiconducting properties, and high transparency to sunlight.[21] Research on the incorporation of transition-metal oxides into Si-based PV and PEC devices is very recent. High work function oxides such as molybdenum oxide, tungsten oxide, vanadium oxide, and cuprous oxide have been explored as hole-selective contacts in silicon solar cells,[22−27] whereas nickel oxide and cobalt oxide have been studied as effective photoanodes for water oxidation.[28−30] Remarkably, defective titanium oxide has also been reported to promote hole transport for efficient water oxidation.[31,32] In contrast, research on transition-metal oxides as electron-selective contacts on crystalline silicon is scarce, with titanium oxide and zinc oxide so far the only transition-metal oxides reported on Si solar cells[33−35] and strontium titanium oxide as Si photocathodes for water reduction.[13]

Although it has not received as much attention yet, tantalum oxide (TaO_x) is a promising material for electron-selective contacts to silicon because of (i) small conduction band offset,[21,36] which allows electrons from the silicon conduction band to flow through TaO_x; (ii) large valence band offset (~2.9 eV),[21,36] which provides a barrier to prevent holes in the silicon valence band from flowing to the oxide and further to the metal cathode; and (iii) recently demonstrated effective passivation of silicon surface defects.[37,38] In addition, TaO_x possesses high thermal and chemical stability under various pH conditions,[39−42] making it a sensible choice for PEC applications. In this work, we report a nanoscale TaO_x film (~6 nm) as a robust passivated electron-selective heterocontact for c-Si based photovoltaics and photoeletrochemical water reduction for the first time, demonstrating significantly improved solar-to-electricity and solar-to-hydrogen conversion efficiencies.

We investigate the optoelectronic properties of TaO_x films synthesized by atomic layer deposition (ALD) and hydrogenated by plasma-enhanced chemical vapor deposited (PECVD) silicon nitride (SiN_x), including core-level, valence band, work function, contact resistivity, and surface passivation properties. We then demonstrate, for the first time, the application of hydrogenated TaO_x to Si-based PV and PEC devices for the generation of electricity and hydrogen, achieving a solar-to-electricity efficiency of 19.1% and applied bias photon-to-current efficiency of 7.7%, which correspond to 2% and 3.8% absolute enhancement, respectively, over control devices without a TaO_x interlayer.

X-ray photoelectron spectroscopy (XPS) was employed to reveal TaO_x electronic properties, including stoichiometry, valence band, and work function, which are critical to the transport of electrons. The results are shown in Figure 1. While

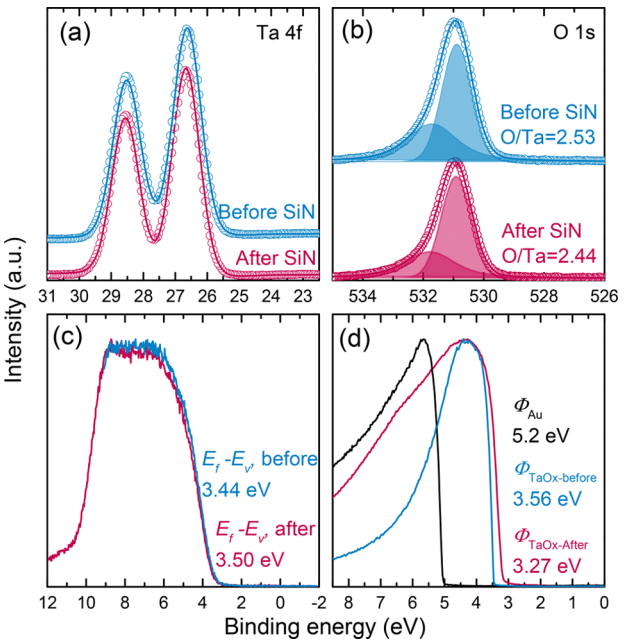

Figure 1. Electronic characterizations of atomic layer deposited TaO_x films before and after hydrogenation. Panels a and b present the core-level spectrum of Ta 4f and O 1s, respectively. Panel c shows the valence band spectrum, and panel d shows the secondary electron cutoff spectrum with a gold (Au) reference.

the Ta 4f spectra shows typical doublet peaks located at 26.5 and 28.5 eV for Ta 4f 7/2 and Ta 4f 5/2, respectively,[43] the O 1s spectra can be fitted with two Gaussian components with peaks positioned at 530.8 and 532 eV, respectively. The small peak located at 532 eV is usually attributed to peroxide O_2^{2-}, although sometimes it can also be due to surface contamination.[43] The component with lower binding energy peaked at 530.8 eV is from Ta−O binding.[43] Notably, the peak positions for both Ta 4f and O 1s are observed to be the same for the TaO_x film before and after SiN_x hydrogenation. However, we can notice a slight reduction in the core level peak areas of O 1s spectra after SiN_x hydrogenation. The extracted TaO_x film stoichiometry based on core level peak areas is also included in Figure 1b. The result shows the as-deposited TaO_x has an O to Ta atomic fraction of 2.53, and the TaO_x after SiN_x hydrogenation has an O to Ta atomic fraction of 2.44, implying the hydrogenation process makes the TaO_x film slightly more substoichiometric.

Figure 1c presents the valence band spectrum of the two TaO_x films, showing no significant difference (<2% change). Although the TaO_x film after SiN_x hydrogenation is more metallic, no defect band in the band gap can be seen, suggesting negligible amount of filled states at the Fermi level. Furthermore, the XPS secondary electron cutoff result shows that the TaO_x film after SiN_x hydrogenation has a work function of 3.27 eV, approximately 0.3 eV lower than that of as-

DOI: 10.1021/acsenergylett.7b01153
ACS Energy Lett. 2018, 3, 125−131

deposited TaO_x. The lower work function can be attributable to the lower cation oxidation state that was revealed by the core level measurements. As proposed in ref 44, the lower cation oxidation state would result in lower work function, because lower oxidation-state cations are less electronegative than higher oxidation-state cations. The measured work function of the TaO_x films is significantly lower than that of TiO_2 presented in the literature (i.e., ~4.2 eV).[45,46] The reduced work function is expected to promote downward band-bending inside the silicon wafer drawing electrons to the surface and consequently improving electron transport.

As mentioned above, TaO_x combines a high valence band offset, creating a potential barrier to hole transport; nevertheless, holes can still flow to the interface between TaO_x and Si, unless it is perfectly passivated. Therefore, the carrier selectivity of an *n*-Si/TaO_x heterostructure needs to be evaluated by characterizing not only the contact resistivity, ρ_c, but also the surface recombination velocity. A highly selective contact is achieved through a simultaneous reduction in recombination and contact resistance. One of the most straightforward techniques to probe the recombination properties of c-Si surfaces is by measuring the effective minority carrier lifetime (τ_{eff}) of symmetrically film-passivated wafers in a contactless fashion,[47] as illustrated in Figure S1 in the Supporting Information.

Figure 2a depicts the quality of surface passivation provided by 6 nm TaO_x films before and after SiN_x hydrogenation by plotting the injection-dependent effective carrier lifetime $\tau_{eff}(\Delta n)$ of *n*-type undiffused c-Si samples. As can be seen, the as-deposited TaO_x film (i.e., before hydrogenation) provides a poor passivation to silicon surfaces, with τ_{eff} of

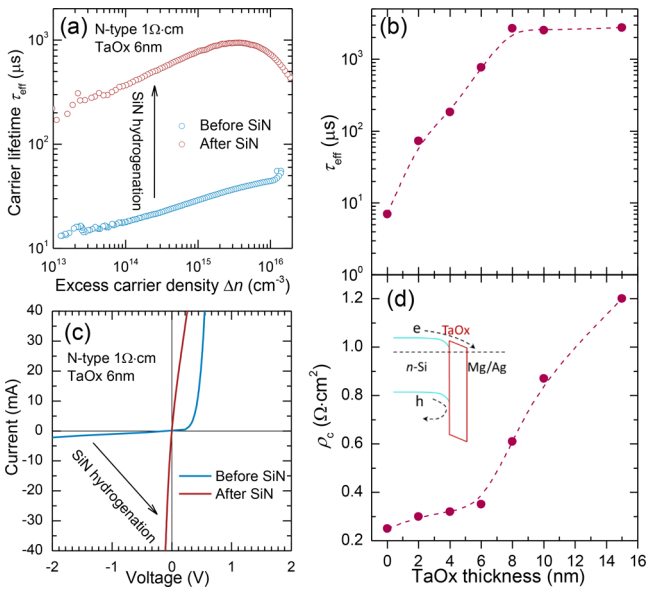

Figure 2. Carrier selectivity characterizations of TaO_x passivated electron heterocontacts to *n*-type c-Si. Panel a presents the effective carrier lifetime τ_{eff} versus excess carrier density Δn for c-Si passivated with TaO_x films before and after SiN_x hydrogenation. Panel b presents the effect of hydrogenated TaO_x film thickness on τ_{eff}. Panel c presents representative *I*−*V* measurements of TaO_x samples before and after SiN_x hydrogenation. Panel d shows the effect of hydrogenated TaO_x film thickness on the contact resistivity ρ_c. The inset in panel d shows a schematic illustration of the band diagram with hydrogenated TaO_x.

~30 μs at an excess carrier density $\Delta n = 10^{15}$ cm^{-3}. The level of surface passivation is improved more than 1 order of magnitude upon a SiN_x hydrogenation treatment, resulting in τ_{eff} as high as ~650 μs at $\Delta n = 10^{15}$ cm^{-3}, corresponding to a recombination current density J_0 of 22.5 fA/cm^2 and an implied open-circuit voltage (V_{OC}) of 690 mV. Figure 2b shows that the passivation quality of hydrogenated TaO_x films depends strongly on the film thickness; the corresponding injection-dependent lifetime curves are shown in detail as Figure S1b. As the TaO_x thickness increases, τ_{eff} first increases and then tends to plateau at 8 nm TaO_x. The highest lifetime achieved at $\Delta n = 10^{15}$ cm^{-3} is ~2.7 ms. The substantial enhancement in passivation upon SiN_x hydrogenation is mainly attributable to the hydrogenation of defects at the TaO_x/c-Si interface during the deposition of SiN_x.[38]

The contact resistivity ρ_c of TaO_x to *n*-type c-Si was measured using the method devised by Cox and Strack.[48] The test structure is schematically depicted in Figure S2a. Low work function metal Mg was employed here to further enhance the electron transport, as demonstrated in previous work.[49] Figure 2c shows a representative *I*−*V* measurement of TaO_x samples before and after the SiN_x hydrogenation treatment. As can be seen, the sample before SiN_x hydrogenation exhibits severe rectifying behavior and a high contact resistivity. By contrast, the contact behavior of the TaO_x (~6 nm) film is enhanced dramatically upon SiN_x hydrogenation, resulting in an Ohmic contact to the *n*-type Si substrate. The full series of *I*−*V* measurements are shown in Figure S2b; from that series, the ρ_c for the heterocontact with ~6 nm hydrogenated TaO_x is determined to be ~0.35 Ω·cm^2, which is sufficiently low to function as a full area heterocontact for *n*-type silicon PV and PEC devices. The good electron transport provided by the hydrogenated TaO_x on *n*-type Si can be attributed to (i) a reduced work function and/or (ii) Fermi-level depinning as a consequence of the passivation of interface states between TaO_x and the silicon substrate. The dependence of contact resistivity on TaO_x thickness is depicted in Figure 2d, exhibiting a slow increase in ρ_c and then a sharp increase when TaO_x is beyond 6 nm. Indeed, when TaO_x thickness exceeds 10 nm, the contact behaves in a rectifying fashion even after the SiN_x hydrogenation. The increasing trend in both τ_{eff} and ρ_c creates a trade-off between surface passivation and contact resistivity provided by the TaO_x film. To resolve this trade-off, we fabricate completed silicon solar cells in order to find the optimum TaO_x film thickness for maximizing the carrier selectivity.

Upon quantifying the carrier selectivity of TaO_x, we can now perform a comparison to state-of-the-art electron-selective contacts reported in the literature. Table S1 in the Supporting Information summarizes the performance parameters of the various electron-selective contacts, including work function, contact resistivity, and recombination current density. Compared to the lowest work function materials, such as alkali and alkaline earth metals or salts, TaO_x itself can provide an effective passivation of the silicon surface, with a recombination current density of just $J_0 \sim 22.5$ fA/cm^2. In contrast, to achieve low recombination in the case of electron-selective contacts based on alkali or alkaline earth metal salts, it is necessary to insert an additional passivation layer, such as amorphous silicon, without significant compromise in the contact resistivity.[50] The surface passivation quality by TaO_x is slightly better than the recently reported SiO_2/TiO_2 stack which has enabled an efficiency of 22.1% silicon solar cells,[51] demonstrat-

DOI: 10.1021/acsenergylett.7b01153
ACS Energy Lett. 2018, 3, 125−131

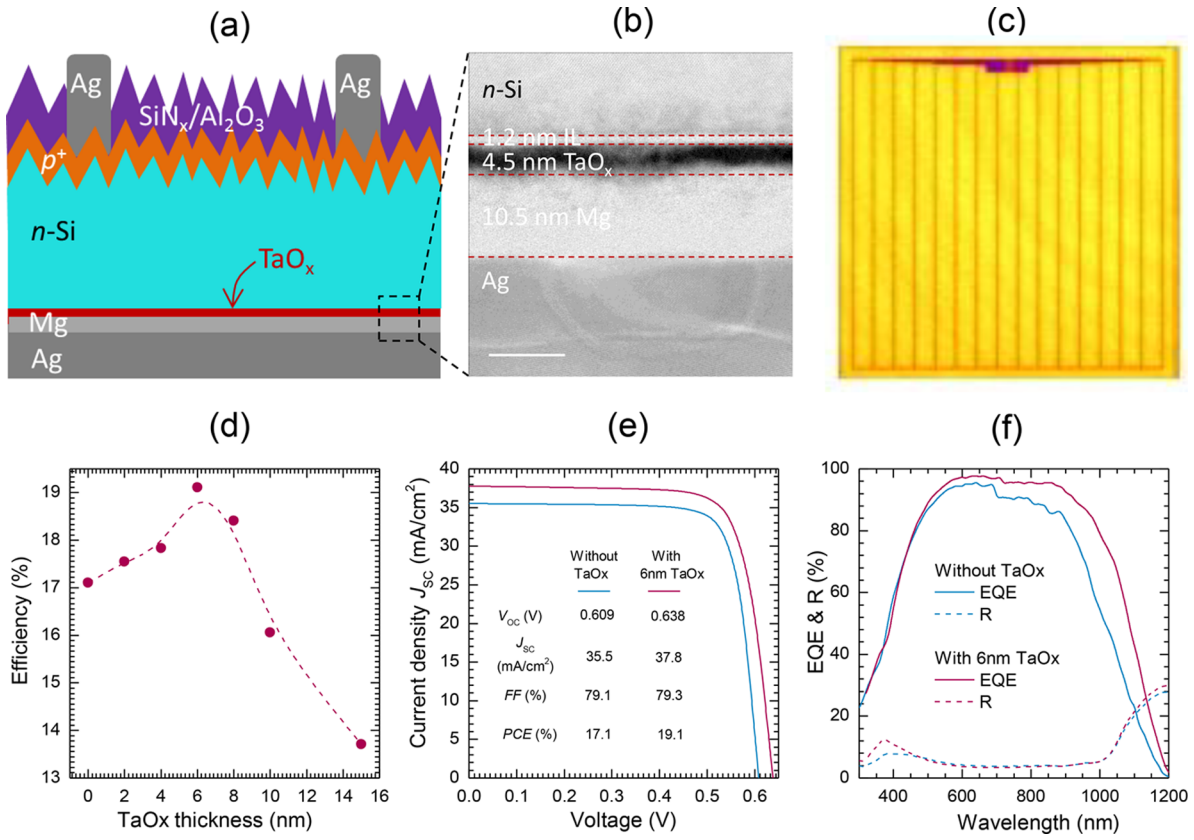

Figure 3. PV device performance with a full-area rear TaO_x passivated electron heterocontact. (a) Schematic cross-section of an *n*-type silicon solar cell featuring a full-area TaO_x/Mg/Ag rear contact. (b) Cross-sectional transmission electron microscopy (TEM) image of the rear heterocontacts. (c) Photoluminescence image of the complete solar cell. (d) Dependence of cell efficiency on TaO_x film thickness. (e) Light *J*–*V* curves and electrical parameters of cells with and without a ~6 nm TaO_x interlayer. (f) Spectral response (external quantum efficiency and reflectance) of the two cells.

ing a high potential to achieve high-efficiency solar cells by using TaO_x-based electron-selective heterocontacts. It is notable, however, that in our experiments it has been necessary to hydrogenate the TaO_x/Si interface by depositing a sacrificial layer of SiN_x; it should be possible, however, to perform such hydrogenation by other simpler means, such as hydrogen plasma treatment.[52] A distinctive feature is that, among all the electron-selective contacts in Table S1, TaO_x exhibits the highest stability against chemical solutions, making it a sensible choice for photoelectrochemical applications.

The complete silicon solar cells feature full area one dimensional TaO_x passivated heterocontacts and are schematically depicted in Figure 3a. Figure 3b presents a cross-sectional transmission electron micrograph of the rear heterocontacts, showing the ~6 nm TaO_x consists of ~1.2 nm interfacial layer and ~4.5 nm TaO_x. The interfacial layer may result from exposure to ambient after deionized water rinse or water precursor during the first few ALD cycles. A photoluminescence image of the complete solar cells (Figure 3c) employing a 1025 nm short-pass filter shows the cell surfaces had uniform optical, passivating, and contact behaviors. Figure 3d shows the solar cell power conversion efficiency as a function of TaO_x film thickness [detailed electrical parameters for these cells (V_{OC}, J_{SC}, and FF) are presented in Figure S3 and Table S2]. As can be seen, the efficiency exhibits a strong dependence on TaO_x film thickness, with a maximum at a thickness of 6 nm. As TaO_x film thickness increases, the efficiency first increases primarily because of an increase in surface passivation quality and therefore an enhancement in V_{OC} and then decreases after 6 nm mainly because of a high contact resistivity imposed by the thicker TaO_x film and therefore a reduction in FF. These solar cells trends are consistent with the carrier selectivity results presented in Figure 2.

The illuminated *J*–*V* curve for the champion cell with 6 nm TaO_x is plotted in Figure 3e, which also includes the reference cell without a TaO_x film. It can be seen that all cell parameters were improved drastically by inserting the 6 nm thick TaO_x layer, yielding a 19.1% solar-to-electricity conversion efficiency, which is 2% absolute higher than the 17.1% reference cell. Compared to the reference cell with metal directly on silicon, an absolute gain of 29 mV in open-circuit voltage was obtained, primarily because of the improved surface passivation provided by the hydrogenated TaO_x film. The suppression of the recombination at rear silicon surfaces also leads to a gain of 2.3 mA/cm^2 in short-circuit current. It is interesting to note that the fill factor is negligibly affected by the insertion of 6 nm TaO_x, despite a slight increase in contact resistivity. It is worth mentioning that the obtained V_{OC} (638 mV) is significantly lower than the implied V_{OC} from the lifetime sample (~690 mV). One tentative cause for this behavior is the damage to surface passivation during Mg metal evaporation, a behavior that has also been observed for the case of amorphous silicon.[49] A possible solution to mitigate this damage would be the use of other low work function materials such as lithium or magnesium fluorides.[16,17] The spectral response plotted in

DOI: 10.1021/acsenergylett.7b01153
ACS Energy Lett. 2018, 3, 125–131

Figure 3f shows a similar reflectance but a significant enhancement in the external quantum efficiency (EQE) at long wavelengths (i.e., range from ~900−1200 nm) for the cell with the TaO_x heterocontact, due to the passivation of the rear surface by the TaO_x layer. This is consistent with the above-mentioned improvements in effective lifetime, voltage, and current and provides additional evidence of the enhancements realized from TaO_x passivation.

Finally, the concept of electron transport by hydrogenated TaO_x is also demonstrated for photoelectrochemical hydrogen evolution. The electron-selective heterocontact was prepared by replacing the Mg/Ag metal stack, which we found not to be chemically stable, with 5 nm Ti metal and 5 nm Pt catalyst on a ~6 nm TaO_x film, to enable stable and efficient hydrogen evolution reactions, as shown in Figure 4a. Ti metal with its

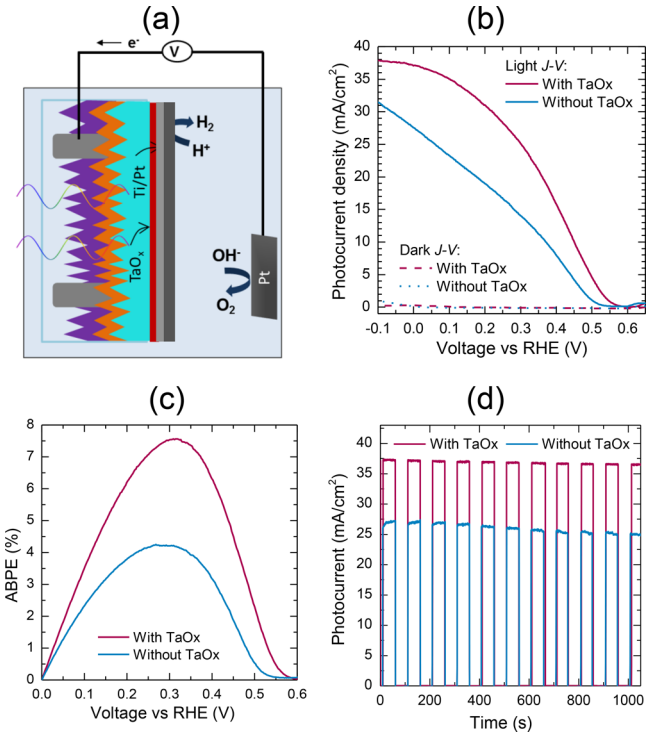

Figure 4. PEC device results with TaO_x passivated electron heterocontacts. Panel a illustrates the schematic of an *n*-type silicon photocathode using TaO_x passivated electron heterocontacts. Panel b presents the photoelectrochemical current−voltage curves of Si photocathodes with and without ~6 nm TaO_x interlayer. Panel c shows applied bias photon-to-current efficiency (ABPE). Panel d shows amperometric current−time curves of Si photocathodes at 0 V vs the reversible hydrogen electrode (RHE).

relatively low work function (~4.2 eV[53]) assists in reducing the barrier between TaO_x and Pt, improving the photovoltage over a device with Pt only.[4] When the silicon device is illuminated, photogenerated minority carriers (holes in this case) flow toward the illuminated p^+ region at the front surface, whereas the majority carriers (electrons in this case) are transported through the TaO_x interlayer to the outer Ti/Pt catalyst, where the hydrogen evolution reaction takes place.

For comparison, a control PEC device was prepared without a TaO_x film. Figure 4b compares the photoelectrochemical performance of these two PEC devices, with and without TaO_x. The control device shows an onset potential of 525 mV for water reduction, whereas the photoelectrode with ~6 nm of TaO_x showed a more positive onset potential of 565 mV. The photocurrent density of the device with a TaO_x passivated electrode reaches 37.1 mA/cm^2 at 0 V vs RHE, compared to the 27.5 mA/cm^2 obtained for the control electrode without TaO_x. The significant enhancement in both photocurrent and photovoltage is consistent with the improved photovoltaic characteristics shown in Figure 3, and can be attributed to the role of TaO_x in suppressing carrier recombination at the rear surface while maintaining efficient electron transport.

To evaluate the improvement in photoelectrochemical performance with TaO_x layer, applied bias photon-to-current efficiency (ABPE) has been calculated using the method reported previously.[54] It is noted that ABPE values derived from three-electrode measurements do not include the losses that might be present at the counter electrode in a two-electrode system. ABPE for TaO_x passivated electrode has been measured to reach 7.7%, which is almost double that of the control electrode without TaO_x interlayer. However, this PEC conversion efficiency is well below the 19.1% achieved by the best photovoltaic device incorporating a TaO_x interlayer, mainly because of lower photovoltage and FF. Beyond the thermodynamic energy loss associated with the water reduction electrolyte, this disparity can be largely attributed to an unfavorable energy band alignment in the Ti/TaO_x/Si photocathode, compared to the Mg/TaO_x/Si contact architecture used in the PV devices. The use of Ti instead of Mg can potentially lead to a higher barrier height for electron transport and therefore cause significant loss in the electron contact resistivity. Nevertheless, these experiments have demonstrated, for the first time, that hydrogentated TaO_x is capable of providing passivation of the silicon surface and, simultaneously, transport efficiently the electrons for PEC water reduction.

As the electrodes used for water splitting must endure a highly corrosive and reducing environment, stability tests have been carried out to evaluate the photoresponse and photostability. As shown in Figure 4d, the reference electrode exhibited a slight drop in photocurrent with time, while the photoelectrode with TaO_x film showed a highly stable photoresponse. It is known that c-Si is stable in acid environments while it is highly unstable in oxidizing conditions. The instability of the control electrode without TaO_x interlayer is likely attributed to the lack of hole-blocking effect at the interface, inducing possible self-oxidizing conditions. The long-term stability of the TaO_x-based electrode is further confirmed in 1 M hydrochloric acid solution for 2 h of continuous operation (see Figure S4).

We have successfully demonstrated a hydrogenated TaO_x (~6 nm) electron-selective heterocontact that simultaneously provides high quality passivation of the silicon surface (i.e., lifetime ~650 μs) and effective transport of electrons (i.e., contact resistivity ~0.35 Ω·cm^2). The XPS measurements revealed the hydrogenation induced by PECVD SiN_x resulted in reduction in TaO_x stoichiometry and work function, making TaO_x film favorable for electron contacts. We have achieved a solar-to-electricity efficiency of 19.1% and a solar-to-hydrogen efficiency of 7.7%, which correspond to a 2% and 3.8% absolute enhancement, respectively, over the control devices without a TaO_x interlayer. These findings related to tantalum oxide are not limited to a silicon-based device platform; more generally, they indicate a generic pathway for interface engineering of optoelectronic and photoelectrochemical applications.

DOI: 10.1021/acsenergylett.7b01153
ACS Energy Lett. 2018, 3, 125−131

EXPERIMENTAL METHODS

The TaO_x films were deposited by a thermal ALD reactor (Picosun, R200 Advanced) using Tantalum Ethoxide precursor at 250 °C and had a corresponding growth rate of 0.35 Å/cycle as measured by ex-situ spectroscopic ellipsometry (J.A. Woolam M2000 ellipsometer). The hydrogenation of TaO_x film was realized by capping PECVD SiN_x atop TaO_x and then stripping off the SiN_x layer by 1% hydrofluoric acid, taking advantage of the exceptional chemical stability of TaO_x film under various pH conditions. PECVD SiN_x has been well-known in providing hydrogen to manipulate bulk and interfacial properties of a range of materials such as silicon.[55] The capping SiN_x layer was deposited in a microwave/radio frequency PECVD reactor (AK400, Roth & Rau),[56] having a thickness of 85 nm and a refractive index of ∼1.9 at 632 nm.

Further experimental details are given in the Supporting Information.

ASSOCIATED CONTENT

Supporting Information

The Supporting Information is available free of charge on the ACS Publications website at DOI: 10.1021/acsenergylett.7b01153.

Characterization methods including X-ray photoelectron spectroscopy, carrier lifetime, and contact resistivity; fabrication and characterization details of silicon PV and PEC devices (PDF)

AUTHOR INFORMATION

Corresponding Author

*E-mail: yimao.wan@anu.edu.au.

ORCID

Yimao Wan: 0000-0003-2999-2464

Author Contributions

Y.W. supervised the project. Y.W. and S.K.K. conceived the idea. Y.W. and C.S. carried out the material development, device fabrication, characterization, and analysis. Y.W., S.K.K., and P.R.N. conducted the water-splitting experiment. J.B. and M.H. assisted with XPS characterization and analysis. D.Y. and J.P. assisted with PV device fabrication and characterization. S.M., H.H.T., C.J., A.J., and A.C. discussed the results. The manuscript was mainly written and revised by Y.W. and S.K.K. All authors commented on the manuscript.

Author Contributions

$^{\nabla}$Y.W. and S.K.K. contributed equally to this work.

Notes

The authors declare no competing financial interest.

ACKNOWLEDGMENTS

This work was supported by the Australian Government through the Australian Research Council (ARC). Some facilities at the Australian National Fabrication Facility and Centre for Advanced Microscopy at ANU were used. XPS characterization was performed at the Joint Center for Artificial Photosynthesis, supported through the Office of Science of the U.S. Department of Energy under Award Number DE-SC0004993. A.J., M.H., and J.B. acknowledge funding from the Bay Area Photovoltaics Consortium (BAPVC).

REFERENCES

(1) Creutzig, F.; Agoston, P.; Goldschmidt, J. C.; Luderer, G.; Nemet, G.; Pietzcker, R. C. The underestimated potential of solar energy to mitigate climate change. *Nature Energy* **2017**, *2*, 17140.

(2) Walter, M. G.; Warren, E. L.; McKone, J. R.; Boettcher, S. W.; Mi, Q.; Santori, E. A.; Lewis, N. S. Solar Water Splitting Cells. *Chem. Rev.* **2010**, *110*, 6446−6473.

(3) Sun, K.; Shen, S.; Liang, Y.; Burrows, P. E.; Mao, S. S.; Wang, D. Enabling Silicon for Solar-Fuel Production. *Chem. Rev.* **2014**, *114*, 8662−8719.

(4) Esposito, D. V.; Levin, I.; Moffat, T. P.; Talin, A. A. H2 evolution at Si-based metal−insulator−semiconductor photoelectrodes enhanced by inversion channel charge collection and H spillover. *Nat. Mater.* **2013**, *12*, 562−568.

(5) Reece, S. Y.; Hamel, J. A.; Sung, K.; Jarvi, T. D.; Esswein, A. J.; Pijpers, J. J. H.; Nocera, D. G. Wireless Solar Water Splitting Using Silicon-Based Semiconductors and Earth-Abundant Catalysts. *Science* **2011**, *334*, 645−648.

(6) Ji, L.; Hsu, H.-Y.; Li, X.; Huang, K.; Zhang, Y.; Lee, J. C.; Bard, A. J.; Yu, E. T. Localized dielectric breakdown and antireflection coating in metal-oxide-semiconductor photoelectrodes. *Nat. Mater.* **2017**, *16*, 127−131.

(7) Zhou, X.; Liu, R.; Sun, K.; Papadantonakis, K. M.; Brunschwig, B. S.; Lewis, N. S. 570 mV photovoltage, stabilized n-Si/CoOx heterojunction photoanodes fabricated using atomic layer deposition. *Energy Environ. Sci.* **2016**, *9*, 892−897.

(8) Zhao, J. Recent advances of high-efficiency single crystalline silicon solar cells in processing technologies and substrate materials. *Sol. Energy Mater. Sol. Cells* **2004**, *82*, 53−64.

(9) Glunz, S.; Feldmann, F.; Richter, A.; Bivour, M.; Reichel, C.; Steinkemper, H.; Benick, J.; Hermle, M. The irresistible charm of a simple current flow pattern - approaching 25% with a solar cell featuring a full-area back contact. In 31st European Photovoltaic Solar Energy Conference and Exhibition, Hamburg, Germany, September, 2015.

(10) Masuko, K.; Shigematsu, M.; Hashiguchi, T.; Fujishima, D.; Kai, M.; Yoshimura, N.; Yamaguchi, T.; Ichihashi, Y.; Mishima, T.; Matsubara, N.; et al. Achievement of More Than 25% Conversion Efficiency With Crystalline Silicon Heterojunction Solar Cell. *Photovoltaics, IEEE Journal of* **2014**, *4*, 1433−1435.

(11) Godfrey, R. B.; Green, M. A. 655 mV open - circuit voltage, 17.6% efficient silicon MIS solar cells. *Appl. Phys. Lett.* **1979**, *34*, 790−793.

(12) Green, M. A.; Blakers, A. W. Advantages of metal-insulator-semiconductor structures for silicon solar cells. *Sol. Cells* **1983**, *8*, 3−16.

(13) Ji, L.; McDaniel, M. D.; Wang, S.; Posadas, A. B.; Li, X.; Huang, H.; Lee, J. C.; Demkov, A. A.; Bard, A. J.; Ekerdt, J. G.; et al. A silicon-based photocathode for water reduction with an epitaxial SrTiO3 protection layer and a nanostructured catalyst. *Nat. Nanotechnol.* **2015**, *10*, 84−90.

(14) Hill, J. C.; Landers, A. T.; Switzer, J. A. An electrodeposited inhomogeneous metal-insulator-semiconductor junction for efficient photoelectrochemical water oxidation. *Nat. Mater.* **2015**, *14*, 1150−1155.

(15) Pourbaix, M. *Atlas of Electrochemical Equilibria in Aqueous Solutions*, 2nd ed.; National Association of Corrosion Engineers: Houston, TX, 1974.

(16) Bullock, J.; Zheng, P.; Jeangros, Q.; Tosun, M.; Hettick, M.; Sutter-Fella, C. M.; Wan, Y.; Allen, T.; Yan, D.; Macdonald, D.; et al. Lithium Fluoride Based Electron Contacts for High Efficiency n-Type Crystalline Silicon Solar Cells. *Adv. Energy Mater.* **2016**, *6*, 1600241.

(17) Wan, Y.; Samundsett, C.; Bullock, J.; Allen, T.; Hettick, M.; Yan, D.; Zheng, P.; Zhang, X.; Cui, J.; McKeon, J.; et al. Magnesium Fluoride Electron-Selective Contacts for Crystalline Silicon Solar Cells. *ACS Appl. Mater. Interfaces* **2016**, *8*, 14671−14677.

(18) Wan, Y.; Samundsett, C.; Bullock, J.; Hettick, M.; Allen, T.; Yan, D.; Peng, J.; Wu, Y.; Cui, J.; Javey, A. Conductive and Stable

DOI: 10.1021/acsenergylett.7b01153
ACS Energy Lett. 2018, 3, 125−131

Magnesium Oxide Electron-Selective Contacts for Efficient Silicon Solar Cells. *Adv. Energy Mater.* **2017**, *7*, 1601863.
(19) Schmidt, J.; Titova, V.; Zielke, D. Organic-silicon heterojunction solar cells: Open-circuit voltage potential and stability. *Appl. Phys. Lett.* **2013**, *103*, 183901.
(20) Zhang, Y.; Zu, F.; Lee, S. T.; Liao, L.; Zhao, N.; Sun, B. Heterojunction with organic thin layers on silicon for record efficiency hybrid solar cells. *Adv. Energy Mater.* **2014**, *4*, 1300923.
(21) Greiner, M. T.; Helander, M. G.; Tang, W.-M.; Wang, Z.-B.; Qiu, J.; Lu, Z.-H. Universal energy-level alignment of molecules on metal oxides. *Nat. Mater.* **2012**, *11*, 76−81.
(22) Battaglia, C.; de Nicolás, S. M.; De Wolf, S.; Yin, X.; Zheng, M.; Ballif, C.; Javey, A. Silicon heterojunction solar cell with passivated hole selective MoOx contact. *Appl. Phys. Lett.* **2014**, *104*, 113902.
(23) Battaglia, C.; Yin, X.; Zheng, M.; Sharp, I. D.; Chen, T.; McDonnell, S.; Azcatl, A.; Carraro, C.; Ma, B.; Maboudian, R.; et al. Hole selective MoO x contact for silicon solar cells. *Nano Lett.* **2014**, *14*, 967−971.
(24) Bivour, M.; Temmler, J.; Steinkemper, H.; Hermle, M. Molybdenum and tungsten oxide: High work function wide band gap contact materials for hole selective contacts of silicon solar cells. *Sol. Energy Mater. Sol. Cells* **2015**, *142*, 34−41.
(25) Bullock, J.; Cuevas, A.; Allen, T.; Battaglia, C. Molybdenum oxide MoOx: A versatile hole contact for silicon solar cells. *Appl. Phys. Lett.* **2014**, *105*, 232109.
(26) Geissbühler, J.; Werner, J.; Martin de Nicolas, S.; Barraud, L.; Hessler-Wyser, A.; Despeisse, M.; Nicolay, S.; Tomasi, A.; Niesen, B.; De Wolf, S.; et al. 22.5% efficient silicon heterojunction solar cell with molybdenum oxide hole collector. *Appl. Phys. Lett.* **2015**, *107*, 081601.
(27) Zhang, X.; Wan, Y.; Bullock, J.; Allen, T.; Cuevas, A. Low resistance Ohmic contact to p-type crystalline silicon via nitrogen-doped copper oxide films. *Appl. Phys. Lett.* **2016**, *109*, 052102.
(28) Chen, L.; Yang, J.; Klaus, S.; Lee, L. J.; Woods-Robinson, R.; Ma, J.; Lum, Y.; Cooper, J. K.; Toma, F. M.; Wang, L.-W.; et al. p-Type Transparent Conducting Oxide/n-Type Semiconductor Heterojunctions for Efficient and Stable Solar Water Oxidation. *J. Am. Chem. Soc.* **2015**, *137*, 9595−9603.
(29) Kenney, M. J.; Gong, M.; Li, Y.; Wu, J. Z.; Feng, J.; Lanza, M.; Dai, H. High-Performance Silicon Photoanodes Passivated with Ultrathin Nickel Films for Water Oxidation. *Science* **2013**, *342*, 836−840.
(30) Sun, K.; Park, N.; Sun, Z.; Zhou, J.; Wang, J.; Pang, X.; Shen, S.; Noh, S. Y.; Jing, Y.; Jin, S.; et al. Nickel oxide functionalized silicon for efficient photo-oxidation of water. *Energy Environ. Sci.* **2012**, *5*, 7872−7877.
(31) Chen, Y. W.; Prange, J. D.; Dühnen, S.; Park, Y.; Gunji, M.; Chidsey, C. E. D.; McIntyre, P. C. Atomic layer-deposited tunnel oxide stabilizes silicon photoanodes for water oxidation. *Nat. Mater.* **2011**, *10*, 539−544.
(32) Hu, S.; Shaner, M. R.; Beardslee, J. A.; Lichterman, M.; Brunschwig, B. S.; Lewis, N. S. Amorphous TiO2 coatings stabilize Si, GaAs, and GaP photoanodes for efficient water oxidation. *Science* **2014**, *344*, 1005−1009.
(33) Allen, T. G.; Bullock, J.; Jeangros, Q.; Samundsett, C.; Wan, Y.; Cui, J.; Hessler-Wyser, A.; De Wolf, S.; Javey, A.; Cuevas, A. A Low Resistance Calcium/Reduced Titania Passivated Contact for High Efficiency Crystalline Silicon Solar Cells. *Adv. Energy Mater.* **2017**, *7*, 1602606.
(34) Avasthi, S.; McClain, W. E.; Man, G.; Kahn, A.; Schwartz, J.; Sturm, J. C. Hole-blocking titanium-oxide/silicon heterojunction and its application to photovoltaics. *Appl. Phys. Lett.* **2013**, *102*, 203901.
(35) Wang, F.; Zhao, S.; Liu, B.; Li, Y.; Ren, Q.; Du, R.; Wang, N.; Wei, C.; Chen, X.; Wang, G.; et al. Silicon solar cells with bifacial metal oxides carrier selective layers. *Nano Energy* **2017**, *39*, 437−443.
(36) Robertson, J.; Chen, C. W. Schottky barrier heights of tantalum oxide, barium strontium titanate, lead titanate, and strontium bismuth tantalate. *Appl. Phys. Lett.* **1999**, *74*, 1168−1170.
(37) Wan, Y.; Bullock, J.; Cuevas, A. Passivation of c-Si surfaces by ALD tantalum oxide capped with PECVD silicon nitride. *Sol. Energy Mater. Sol. Cells* **2015**, *142*, 42−46.
(38) Wan, Y.; Bullock, J.; Cuevas, A. Tantalum oxide/silicon nitride: A negatively charged surface passivation stack for silicon solar cells. *Appl. Phys. Lett.* **2015**, *106*, 201601.
(39) Anderson, M. D.; Aitchison, B.; Johnson, D. C. Corrosion Resistance of Atomic Layer Deposition-Generated Amorphous Thin Films. *ACS Appl. Mater. Interfaces* **2016**, *8*, 30644−30648.
(40) Li, C.; Wang, T.; Luo, Z.; Zhang, D.; Gong, J. Transparent ALD-grown Ta2O5 protective layer for highly stable ZnO photoelectrode in solar water splitting. *Chem. Commun.* **2015**, *51*, 7290−7293.
(41) Chen, S.; Wang, L.-W. Thermodynamic Oxidation and Reduction Potentials of Photocatalytic Semiconductors in Aqueous Solution. *Chem. Mater.* **2012**, *24*, 3659−3666.
(42) Hu, S.; Lewis, N. S.; Ager, J. W.; Yang, J.; McKone, J. R.; Strandwitz, N. C. Thin-Film Materials for the Protection of Semiconducting Photoelectrodes in Solar-Fuel Generators. *J. Phys. Chem. C* **2015**, *119*, 24201−24228.
(43) Atanassova, E.; Spassov, D. X-ray photoelectron spectroscopy of thermal thin Ta2O5 films on Si. *Appl. Surf. Sci.* **1998**, *135*, 71−82.
(44) Greiner, M. T.; Chai, L.; Helander, M. G.; Tang, W.-M.; Lu, Z.-H. Transition Metal Oxide Work Functions: The Influence of Cation Oxidation State and Oxygen Vacancies. *Adv. Funct. Mater.* **2012**, *22*, 4557−4568.
(45) Imanishi, A.; Tsuji, E.; Nakato, Y. Dependence of the Work Function of TiO2 (Rutile) on Crystal Faces, Studied by a Scanning Auger Microprobe. *J. Phys. Chem. C* **2007**, *111*, 2128−2132.
(46) Peng, J.; Duong, T.; Zhou, X.; Shen, H.; Wu, Y.; Mulmudi, H. K.; Wan, Y.; Zhong, D.; Li, J.; Tsuzuki, T. Efficient Indium-Doped TiOx Electron Transport Layers for High-Performance Perovskite Solar Cells and Perovskite-Silicon Tandems. *Adv. Energy Mater.* **2017**, *7*, 1601768.
(47) Sinton, R. A.; Cuevas, A. Contactless determination of current–voltage characteristics and minority-carrier lifetimes in semiconductors from quasi-steady-state photoconductance data. *Appl. Phys. Lett.* **1996**, *69*, 2510−2512.
(48) Cox, R. H.; Strack, H. Ohmic contacts for GaAs devices. *Solid-State Electron.* **1967**, *10*, 1213−1218.
(49) Wan, Y.; Samundsett, C.; Yan, D.; Allen, T.; Peng, J.; Cui, J.; Zhang, X.; Bullock, J.; Cuevas, A. A magnesium/amorphous silicon passivating contact for n-type crystalline silicon solar cells. *Appl. Phys. Lett.* **2016**, *109*, 113901.
(50) Bullock, J.; Hettick, M.; Geissbühler, J.; Ong, A. J.; Allen, T.; Sutter-Fella, C. M.; Chen, T.; Ota, H.; Schaler, E. W.; Wolf, S. D. Efficient silicon solar cells with dopant-free asymmetric heterocontacts. *Nature Energy* **2016**, *1*, 15031.
(51) Yang, X.; Weber, K.; Hameiri, Z.; De Wolf, S. Industrially feasible, dopant-free, carrier-selective contacts for high-efficiency silicon solar cells. *Prog. Photovoltaics* **2017**, *25*, 896−904.
(52) Descoeudres, A.; Barraud, L.; De Wolf, S.; Strahm, B.; Lachenal, D.; Guerin, C.; Holman, Z. C.; Zicarelli, F.; Demaurex, B.; Seif, J.; et al. Improved amorphous/crystalline silicon interface passivation by hydrogen plasma treatment. *Appl. Phys. Lett.* **2011**, *99*, 123506−3.
(53) Sze, S. M.; Ng, K. K. *Physics of Semiconductor Devices*; John Wiley & Sons: Hoboken, NJ, 2006.
(54) Boettcher, S. W.; Warren, E. L.; Putnam, M. C.; Santori, E. A.; Turner-Evans, D.; Kelzenberg, M. D.; Walter, M. G.; McKone, J. R.; Brunschwig, B. S.; Atwater, H. A.; et al. Photoelectrochemical Hydrogen Evolution Using Si Microwire Arrays. *J. Am. Chem. Soc.* **2011**, *133*, 1216−1219.
(55) Aberle, A. G. Overview on SiN surface passivation of crystalline silicon solar cells. *Sol. Energy Mater. Sol. Cells* **2001**, *65*, 239−248.
(56) Wan, Y.; McIntosh, K. R.; Thomson, A. F. Characterisation and optimization of PECVD SiNx as an antireflection coating and passivation layer for silicon solar cells. *AIP Adv.* **2013**, *3*, 032113.

DOI: 10.1021/acsenergylett.7b01153
ACS Energy Lett. 2018, 3, 125−131

Supporting Information:

Tantalum Oxide Electron-Selective Heterocontacts for Silicon Photovoltaics and Photoelectrochemical Water Reduction

Yimao Wan[*†1,2,3], *Siva Krishna Karuturi*[†4], *Christian Samundsett*[1], *James Bullock*[2,3], *Mark Hettick*[2,3], *Di Yan*[1], *Jun Peng*[1], *Parvathala Reddy Narangari*[4], *Sudha Mokkapati*[5], *Hark Hoe Tan*[4], *Chennupati Jagadish*[4], *Ali Javey*[2,3], *and Andres Cuevas*[1]

[1] Research School of Engineering, The Australian National University (ANU), Canberra, ACT 0200, Australia

[2] Department of Electrical Engineering and Computer Sciences, University of California, Berkeley, California 94720, USA

[3] Materials Sciences Division, Lawrence Berkeley National Laboratory, Berkeley, California 94720, USA

[4] Department of Electronic Materials Engineering, Australian National University (ANU), Canberra, ACT 0200, Australia

[5] School of Physics and Astronomy, Cardiff University, Cardiff, Wales, UK

*** Corresponding Author** yimao.wan@anu.edu.au

[†]These authors contributed equally to this work.

X-ray photoelectron spectroscopy (XPS)

XPS was performed using a Kratos AXIS Ultra DLD system, under ultrahigh vacuum with an Al Kα source. An X-ray monochromator was used for all measurements, with electron cut-off and valence band measurements also performed with X-ray excitation. Work function measurements were performed after sputter thinning the Al capping layer to < 5 nm, and a 9 V bias was applied and subsequently subtracted from the final data to aid in collection of cut-off electrons. Voigt lineshapes were used to fit core level spectra, and film stoichiometry was extracted based on the resulting peak areas. A gold reference was used in the same session to verify instrument work function, and to provide a reference for the work functions reported.

Carrier lifetime

One of the most straightforward techniques to probe the recombination properties of c–Si surfaces is by measuring the effective minority carrier lifetime (τ_{eff}) of symmetrically film-coated wafers. This approach is simple, contactless and extremely sensitive to bulk and surface defects. The effective carrier lifetime τ_{eff} as a function of excess carrier density Δn was measured using a Sinton Instruments WCT-120 photo–conductance tool, as illustrated in Figure S1(a). Symmetrical lifetime samples were fabricated on undiffused 1.0 Ω·cm *n*-type float-zone (FZ) grown and {100} oriented crystalline silicon wafers (200 µm). The undiffused wafers were etched in tetramethylammonium hydroxide (TMAH, 25 wt%) at ~ 85 °C to remove saw damage. All samples were then cleaned by the RCA (Radio Corporation of America) procedure and dipped in 1% diluted HF acid to remove any remaining oxide prior to TaO_x deposition and SiN_x capping. The capping SiN_x layers were deposited in a microwave/radio-frequency PECVD reactor (AK400, Roth & Rau). The capping SiN_x has a thickness of 85 nm and a refractive index of 1.9 at 632 nm.

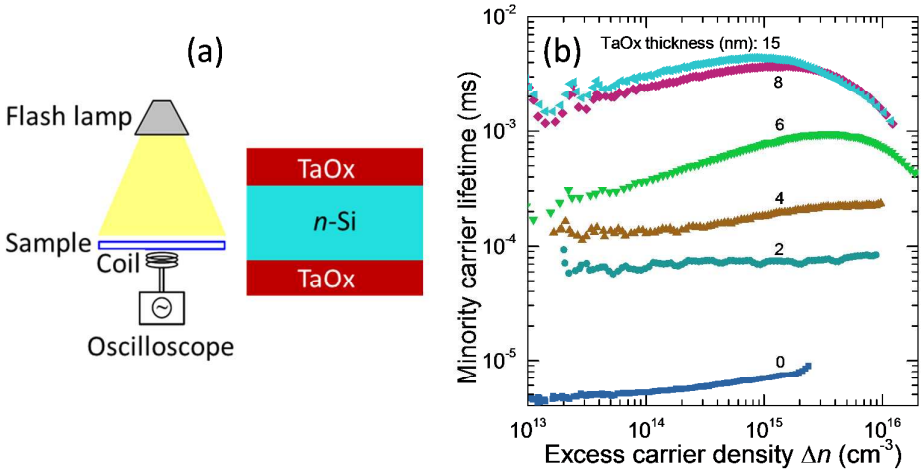

Figure S1: Characterization of effective carrier lifetime. (a) shows the schematic of the lifetime measurements using a Sinton Instruments WCT-120 photo–conductance tool and lifetime test structure. (b)

shows the measured effective carrier lifetime as a function of excess carrier density for *n*-type crystalline silicon wafers symmetrically passivated with TaOx films, with different TaO_x film thickness.

Contact resistivity

The *n*-Si/TaO_x electron-selective contacts were fabricated on planar Czochralski (Cz) *n*-type c-Si wafers with a resistivity of ~1 Ωcm and a thickness of ~250 μm. Samples were subjected to a dilute HF dip prior to deposition of TaO_x films with a variety of thicknesses. An array of circular pads with different diameters was evaporated on the front of the test structures via a shadow mask. Here we used Mg for the front metal, taking advantage of its low work function, and capped it with an outer Ag layer to protect the Mg . A full area Al (~300 nm) metal was evaporated on the rear surface of the contact samples. The rear of the silicon wafer was heavily diffused with phosphorus dopant (n^+) to minimize the contribution of the rear metal/semiconductor contact. Current–voltage (I–V) measurements were taken at room temperature using a Keithley 2425 source–meter. The resistance versus diameter trend was fitted with a spreading resistance model, allowing accurate extraction of contact resistance ρ_c.

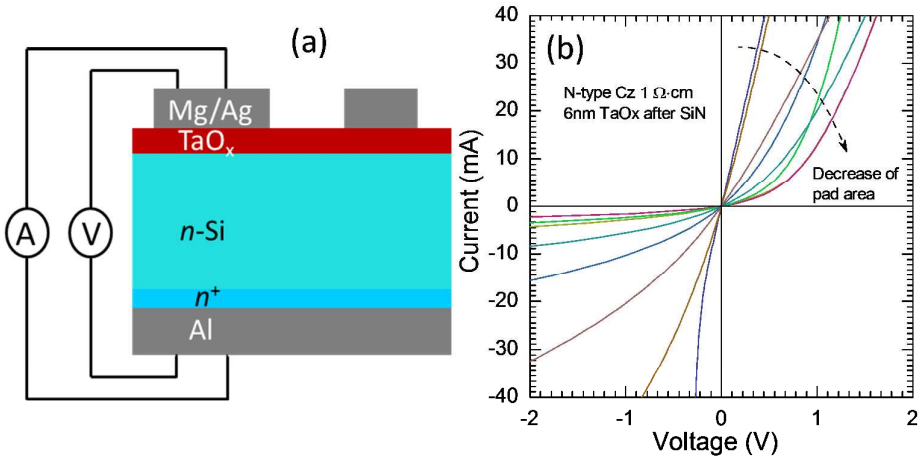

Figure S2: Characterization of contact resistance. (a) shows the schematic of the contact resistivity test structure with TaO_x film. (b) presents a series of I–V measurements of samples with 6 nm TaO_x interlayer between outer metal layers and *n*-type c-Si.

Table S1: Comparison to the state-of-the-art electron selective contacts

Contact materials	Work function (ev)	ρ_c (mΩ·cm^2)	J_0 (fA/cm^2)	Ref.
Ca/Al	2.9	2	~10^6	1
Mg/Al	3.7	220	~10^6	2
LiFx/Al	2.9	1	~10^4	3, 4
MgFx/Al	3.5	35	~10^4	5
MgOx/Al	4.1	17.5	~10^3	6
ZnO:B/Ag	-	40	~200	7
SiO2/TiO2/Al	4.1	300	35	8
TaOx/Mg	3.27	350	22.5	This work

Photovoltaic cells

Proof-of-concept solar cells were fabricated on float-zoned *n*-type c-Si wafers with a resistivity of ~1.0 Ωcm and a thickness of ~180 µm. The textured front silicon surface with random pyramids was formed in an alkaline solution of TMAH, dissolved silicon, IPA and DI water at 85 °C for 60 mins, followed by a boron diffusion (~100 Ω/□) to form a *pn* junction and then by a stack of antireflection and passivation layers of a ~20 nm ALD Al_2O_3 and ~65 nm PECVD SiN_x. The bare silicon surfaces at the rear were then coated with the novel hydrogenated TaO_x passivated heteroelectrodes. Finally, the front surfaces were patterned and metallized with grid of 10 µm width lines and 1.3 mm pitch through photolithography, and then thermal evaporation of a Cr (~10 nm) / Pd (~10 nm) / Ag (~100 nm) stack, and finally thickened by Ag electroplating. The light *J–V* behaviour was measured by a solar simulator from Sinton Instruments under standard one sun conditions (100 mW/cm^2, AM1.5 spectrum, 25 °C)., calibrated with a certified Fraunhofer CalLab reference cell.

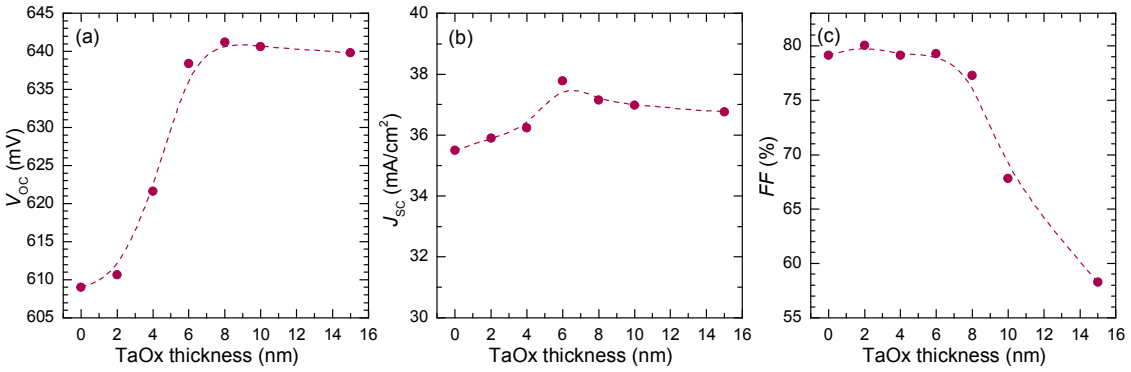

Figure S3: Effect of TaO_x thickness on silicon PV device parameters (a) open-circuit voltage (V_{OC}), (b) short-circuit current (J_{SC}), and (c) fill-factor (*FF*).

Table S2: Summary of silicon PV device parameters

TaOx thickness (nm)	J_{SC} (mA/cm^2)	V_{OC} (mV)	*FF* (%)	η (%)
0	35.50	609.0	79.15	17.11
2	35.90	610.6	80.03	17.55
4	36.24	621.6	79.14	17.83
6	37.77	638.4	79.27	19.11
8	37.15	641.2	77.26	18.41
10	36.98	640.6	67.79	16.06
15	36.76	639.8	58.28	13.71

Photoelectrochemical reaction

To test the PEC performance, photoelectrodes were prepared by replacing the bottom Mg/Ag metal layers of the PV device with a Ti/Pt film. The bilayer film consisting of 5 nm Ti and 5 nm Pt was deposited using an electron beam evaporator (Temescal BJD-2000). Metal wires were attached to the Ag busbar on the front metal grid side using Ag paste. The light harvesting side was sealed with a glass slide using epoxy to protect it from the electrolyte while the catalytically-active back surface coated with Pt was exposed in the electrolyte. Linear sweep voltammetry (LSV) characterizations were performed using a potentiostat (Autolab PGSTAT302N) in a three electrodes setup using Ag/AgCl as reference electrode and Pt as a counter electrode in 1M HCl solution under AM1.5 illumination. The electrode potential versus the Ag/AgCl was converted to reversible hydrogen electrode (RHE) potential according to the Nernst equation: $E_{RHE} = E_{Ag/AgCl} + 0.059\ pH + E^{o}_{Ag/AgCl}$, where E_{RHE} is the converted potential vs. RHE, $E^{o}_{Ag/AgCl}$ = 0.1976 V at 25 °C, and $E_{Ag/AgCl}$ is the experimental potential measured against the Ag/AgCl reference electrode. Photocurrent stability tests were carried out by measuring the photocurrent produced under chopped light irradiation (light/dark cycles of 50 s) at a fixed bias of 0 V versus RHE. The current-voltage results from LSV measurements are converted to applied-bias photon-to-current efficiency using the previously reported method.

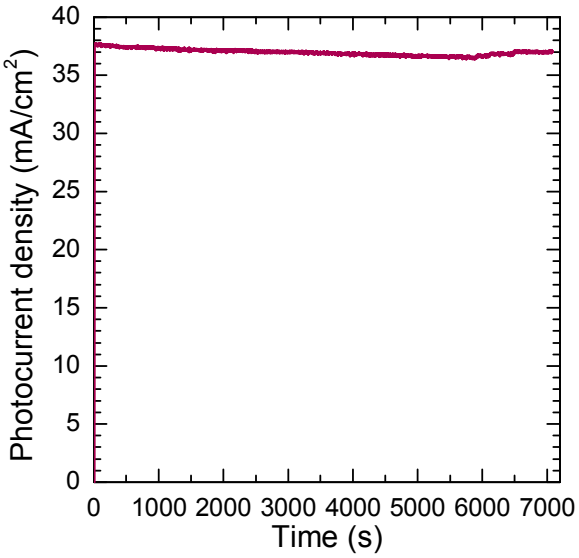

Figure S4: Photoelectrochemical stability of TaO_x passivated heteroelectrode at 0V vs the reversible hydrogen electrode (RHE). The long-term stability of TaO_x is evaluated in 1M hydrochloric acid solution for 2 hours of continuous operation.

References

(1) Allen, T. G.; Bullock, J.; Jeangros, Q.; Samundsett, C.; Wan, Y.; Cui, J.; Hessler-Wyser, A.; De Wolf, S.; Javey, A.; Cuevas, A. A Low Resistance Calcium/Reduced Titania Passivated Contact for High Efficiency Crystalline Silicon Solar Cells. *Advanced Energy Materials* **2017,** *7*, 1602606.

(2) Wan, Y.; Samundsett, C.; Yan, D.; Allen, T.; Peng, J.; Cui, J.; Zhang, X.; Bullock, J.; Cuevas, A. A magnesium/amorphous silicon passivating contact for n-type crystalline silicon solar cells. *Applied Physics Letters* **2016,** *109*, 113901.

(3) Bullock, J.; Zheng, P.; Jeangros, Q.; Tosun, M.; Hettick, M.; Sutter-Fella, C. M.; Wan, Y.; Allen, T.; Yan, D.; Macdonald, D., et al. Lithium Fluoride Based Electron Contacts for High Efficiency n-Type Crystalline Silicon Solar Cells. *Advanced Energy Materials* **2016,** *6*, 1600241.

(4) Bullock, J.; Hettick, M.; Geissbühler, J.; Ong, A. J.; Allen, T.; Sutter-Fella, C. M.; Chen, T.; Ota, H.; Schaler, E. W.; Wolf, S. D., et al. Efficient silicon solar cells with dopant-free asymmetric heterocontacts. *Nature Energy* **2016,** *1*.

(5) Wan, Y.; Samundsett, C.; Bullock, J.; Allen, T.; Hettick, M.; Yan, D.; Zheng, P.; Zhang, X.; Cui, J.; McKeon, J., et al. Magnesium Fluoride Electron-Selective Contacts for Crystalline Silicon Solar Cells. *ACS Applied Materials & Interfaces* **2016,** *8*, 14671-14677.

(6) Wan, Y.; Samundsett, C.; Bullock, J.; Hettick, M.; Allen, T.; Yan, D.; Peng, J.; Wu, Y.; Cui, J.; Javey, A., et al. Conductive and Stable Magnesium Oxide Electron-Selective Contacts for Efficient Silicon Solar Cells. *Advanced Energy Materials* **2017,** *7*, 1601863-n/a.

(7) Wang, F.; Zhao, S.; Liu, B.; Li, Y.; Ren, Q.; Du, R.; Wang, N.; Wei, C.; Chen, X.; Wang, G., et al. Silicon solar cells with bifacial metal oxides carrier selective layers. *Nano Energy* **2017,** *39*, 437-443.

(8) Yang, X.; Bi, Q.; Ali, H.; Davis, K.; Schoenfeld, W. V.; Weber, K. High-Performance TiO2-Based Electron-Selective Contacts for Crystalline Silicon Solar Cells. *Advanced Materials* **2016,** *28*, 5891-5897.